

CrystEngComm

Accepted Manuscript



This is an *Accepted Manuscript*, which has been through the Royal Society of Chemistry peer review process and has been accepted for publication.

Accepted Manuscripts are published online shortly after acceptance, before technical editing, formatting and proof reading. Using this free service, authors can make their results available to the community, in citable form, before we publish the edited article. We will replace this *Accepted Manuscript* with the edited and formatted *Advance Article* as soon as it is available.

You can find more information about *Accepted Manuscripts* in the [Information for Authors](#).

Please note that technical editing may introduce minor changes to the text and/or graphics, which may alter content. The journal's standard [Terms & Conditions](#) and the [Ethical guidelines](#) still apply. In no event shall the Royal Society of Chemistry be held responsible for any errors or omissions in this *Accepted Manuscript* or any consequences arising from the use of any information it contains.

Cite this: DOI: 10.1039/c0xx00000x

www.rsc.org/xxxxxx

ARTICLE TYPE

KF-mediated controlled-synthesis of potassium ytterbium fluorides (doped with Er³⁺) with phase-dependent upconversion luminescence

Mingye Ding,^a Fei Zhu,^a Danyang Ma,^a Xiaoyong Huang,^{*b} Peng Liu,^c Kaixin Song,^c Jiasong Zhong,^a Junhua Xi,^a Zhenguo Ji,^a Daqin Chen^{*a}

Received (in XXX, XXX) Xth XXXXXXXXXX 20XX, Accepted Xth XXXXXXXXXX 20XX

DOI: 10.1039/b000000x

Abstract

Potassium ytterbium fluorides with predictable crystal phases and architectures, such as KYb₃F₁₀ nanoparticles, KYb₂F₇ sub-microplates, 10 microrods, KYbF₄ microplates, micro-bipyramids, K₂YbF₅ microprisms and microrods have been successfully synthesized by simply tuning the molar ratio of KF to Yb³⁺ via a facile and general solution-based route. The influence of the KF dosage on phase and morphology evolution of potassium ytterbium fluorides has been systematically investigated and discussed. And the mechanism about how KF/Yb³⁺ molar ratio influences the anisotropic growth and phase, morphology evolution was proposed. Taking K₂YbF₅ microrods as an example, the possible formation mechanism was presented on the basis of XRD patterns and the corresponding SEM images of the 15 intermediate products obtained at different reaction time intervals. Additionally, the upconversion luminescence properties of Er³⁺ ions (2 mol%) doped potassium ytterbium fluorides with different crystalline phases and architectures were studied in detail. Importantly, this study may provide a great opportunity for systematic study of the general synthesis and luminescence properties of potassium ytterbium fluorides with predictable crystal phases and well-defined morphologies, which can offer a reference for the precisely controlled synthesis of other rare earth fluoride compounds.

1 Introduction

Currently, the precisely architectural manipulation of inorganic functional nano- and micro-materials with controllable morphologies has attracted considerable attention, not only because of fundamental scientific interest but also because of their potential applications in developing novel phosphors and building new optoelectronic devices.¹⁻⁵ It is generally known that the physical, chemical, magnetic and catalytic properties of materials are closely related to their geometrical factors including morphology, size and dimensionality. Hence, 25 developing a synthetic method for simultaneous control over morphology, size and phase purity of inorganic crystals has been becoming the research focus and one of the challenging and urgent tasks. Until now, many efforts have been devoted to exploring excellent approaches to the synthesis of a variety of inorganic functional materials in order to optimize their performance in currently existing applications.⁶⁻¹¹ However, considering the complexity of crystal structures and compositions of inorganic crystals, it is still a big challenge for us to precisely manipulate and control the shape, size and crystal phase of various nano- and micro-materials. Therefore, 30 establishing the relationship between the complex phenomena of crystal growth with the underlying fundamental principles and theories is very necessary for us to develop an efficient strategy for controllable synthesis of inorganic functional crystals.

Lanthanide ions doped upconversion (UC) luminescent materials, which can convert two or more low-energy photons into higher energy photon through an UC process, have attracted considerable attention due to their potential applications in the fields of solid-state lasers, optical communications, three-dimension displays, solar cells, photocatalysis, sensors and nanoscale biolabels.¹²⁻¹⁸ Until now, a 35 variety of UC compounds, such as oxides, oxyfluorides, fluorides, phosphates and sulfides, have been extensively studied.¹⁹⁻²³ Among them, rare earth (RE) fluorides, possessing low photon energy, low nonradiative decay rate, high radiative decay rate and high chemical stability, have been regarded as excellent hosts for performing multicolor UC luminescence.^{24, 25} Although hexagonal NaYF₄ (β-NaYF₄)

is now considered to be one of the most efficient UC hosts, it is still necessary for us to explore and investigate other complex fluorides with improved UC luminescence properties. Recently, Liu's group has demonstrated an alternative approach for enhancing UC emission in $\text{KYb}_2\text{F}_7:\text{Er}^{3+}$ nanocrystals via excitation energy clustering at subunit-cell level, also indicating the necessity and importance of our work.²⁶

Compared with the successful synthesis and applications of KREF_4 , LiREF_4 and REF_3 , little attention has been focused on the preparation of other important RE fluorides. As a class of excellent efficient host materials for UC emissions, potassium ytterbium fluorides including KYbF_4 , $\text{KYb}_3\text{F}_{10}$, KYb_2F_7 and K_2YbF_5 , have attracted more and more attention. The crystal structures of potassium ytterbium fluorides reportedly exhibit three polymorphs: cubic ($\text{KYb}_3\text{F}_{10}$), hexagonal (KYbF_4) and orthorhombic (KYb_2F_7 and K_2YbF_5), depending on synthetic methods and conditions. Up to now, many efforts have been devoted to the chemical synthesis of potassium ytterbium fluorides nano/microcrystals, including hydrothermal method, liquid-solid-solution methodology, coprecipitation method and so on.²⁷⁻³⁰ Most of the reported studies are preponderantly focused on the preparation of KYbF_4 and $\text{KYb}_3\text{F}_{10}$ nanocrystals with different morphologies. However, to the best of our knowledge, there is no report concerning the systematical study of the general synthesis and luminescence properties of potassium ytterbium fluorides crystals with predictable crystal phases and well-defined morphologies.

Herein, we report a facile and general solution-based approach for the controllable synthesis of potassium ytterbium fluorides nano-/microstructures with different crystal phases and various well-defined shapes by simply tuning the molar ratio of KF to Yb^{3+} . As the focus of this paper, we aim to investigate how a precise control over the crystal phases and morphologies of the as-synthesized samples can be achieved through the simple manipulation of the KF/Yb^{3+} molar ratio. Taking K_2YbF_5 microrods as an example, the morphological evolution and possible formation mechanism are also proposed. More importantly, the mechanism of how the KF dosage governs the crystal phase and shape evolution of potassium ytterbium fluorides nano-/microcrystals has been systematically studied and discussed. Moreover, the UC luminescence properties of the as-synthesized potassium ytterbium fluorides (doped with Er^{3+}) nano-/microcrystals with different phases and morphologies are investigated in detail.

2 Experimental section

2.1 Chemicals and Materials: $\text{YbCl}_3 \cdot 6\text{H}_2\text{O}$ (99.99%), $\text{ErCl}_3 \cdot 6\text{H}_2\text{O}$ (99.9%) were purchased from Beijing Founde Star Science & Technology Co., Ltd (China). KOH (85%), $\text{KF} \cdot 2\text{H}_2\text{O}$ (99%), 1-octadecene (90%), and oleic acid (90%) were purchased from Sinopharm Chemical Reagent. All of the chemical reagents were used as starting materials without further purification.

2.2 Synthesis: In a typical experiment, 37.5 mmol KOH was first dissolved in 7.5 mL deionized water, followed by addition of 25 mL ethanol and 25 mL oleic acid under vigorous stirring. Thereafter, 5 mL aqueous solution containing different amounts of $\text{KF} \cdot 2\text{H}_2\text{O}$ (6, 10, 20, 25, 30, 40, 80, 100, 120 mmol) was added to form a turbid mixture. After vigorous stirring for 10 min, 10 mL aqueous solution containing 2 mmol $\text{YbCl}_3 \cdot 6\text{H}_2\text{O}$ was added into the above solution. After additional agitation for 20 min, the resulting mixture was then transferred into a 100-mL Teflon-lined autoclave and heated to 220 °C for 24 h. After cooling down to room temperature, the reaction product was separated by centrifugation, washed with deionized water and ethanol in sequence, and then dried in air at 80 °C for 12 h. For UC luminescence, Er^{3+} ions doped potassium ytterbium fluorides were synthesized in a similar procedure by adding corresponding $\text{ErCl}_3 \cdot 6\text{H}_2\text{O}$ into the precursor mixture.

2.3 Characterization: Powder X-ray diffraction (XRD) measurements were performed on a ARL X' TRA diffractometer at a scanning rate of 10 °/min in the 2 θ range from 10° to 80° with $\text{Cu K}\alpha_1$ radiation ($\lambda=0.15406$ nm). SEM micrographs were obtained using a scanning electron transmission microscope (SEM, JSM-6460, JEOL). TEM images were recorded on JEM-200CX with a field emission gun operating at 200 kV. Images were acquired digitally on a Gatan multiple CCD camera. UC emission spectra were recorded with an Edinburgh Instruments FS5 fluorescence spectrophotometer equipped with an adjustable 980 nm laser diode Module (MDL-III-980-1W, China) as excitation source. UC decay curves were measured with a customized UV to mid-infrared steady-state and phosphorescence lifetime spectrometer (FSP920-C, Edinburgh) equipped with a digital oscilloscope (TDS3052B, Tektronix) and a tunable mid-band OPO pulse laser as excitation source (410-2400 nm, 10 Hz, pulse width ≤ 5 ns, Vibrant 355II, OPOTEK). All the measurements were performed at room temperature.

Cite this: DOI: 10.1039/c0xx00000x

www.rsc.org/xxxxxx

ARTICLE TYPE

3 Results and Discussion

3.1 Structures and Morphologies

Here, we mainly stress the important influence of the KF/Yb^{3+} molar ratios on the crystal phases and morphologies of the final products in our current synthesis. The composition and crystallographic phase purity of the as-prepared products are first examined by XRD technique. Fig. 1 shows the XRD patterns of the samples obtained at different molar ratios of KF to Yb^{3+} as well as the standard data of cubic $\text{KYb}_3\text{F}_{10}$, orthorhombic KYb_2F_7 , hexagonal KYbF_4 and orthorhombic K_2YbF_5 for comparison. As shown, the as-synthesized samples exhibit distinctly different XRD patterns by varying the KF dosage. It can be found that the diffraction peaks of the product prepared with 3:1 $\text{KF}:\text{Yb}^{3+}$ can be well indexed to pure cubic $\text{KYb}_3\text{F}_{10}$ (JCPDS No. 77-2204) (Fig. 1a). The crystal structure of cubic phase is determined with lattice parameters of $a = b = c = 11.431 \text{ \AA}$, space group of $Fm\bar{3}m$.²⁷ Upon a further increase of KF/Yb^{3+} molar ratios, from 5 to 12.5, the well-defined diffraction peaks can be assigned readily to the orthorhombic phase of KYb_2F_7 (JCPDS No. 27-0459) (Fig. 1b-d), which belongs to the orthorhombic crystal system with the $\text{Pna}21$ space group ($a = 11.716 \text{ \AA}$, $b = 13.241 \text{ \AA}$, $c = 7.739 \text{ \AA}$).²⁶ With the increase of $\text{KF}:\text{Yb}^{3+}$ molar ratios, up to 15:1 and 20:1, pure hexagonal KYbF_4 can be successfully synthesized (Fig. 1e-f). The XRD results indicate that the diffraction peaks are in good accordance with hexagonal structure (space group: $\text{P}321$, $a = b = 13.977 \text{ \AA}$, $c = 10.081 \text{ \AA}$) known from literature data (JCPDS No. 28-0850).²⁸ At a wide $\text{KF}:\text{Yb}^{3+}$ molar ratio range condition from 40 to 60, all X-ray diffraction peaks of samples coincide well with the standard data of K_2YbF_5 (JCPDS No. 28-0850). Indexing of the diffraction profile reveals a orthorhombic unit cell with $a = 6.592 \text{ \AA}$, $b = 7.221 \text{ \AA}$, $c = 10.764 \text{ \AA}$ and space group of $\text{Pc}21n$.³⁰ Based on the above results, it can be concluded that the crystal evolves from cubic $\text{KYb}_3\text{F}_{10}$, orthorhombic KYb_2F_7 to hexagonal KYbF_4 and ultimately to orthorhombic K_2YbF_5 with the increase of KF/Yb^{3+} molar ratio.

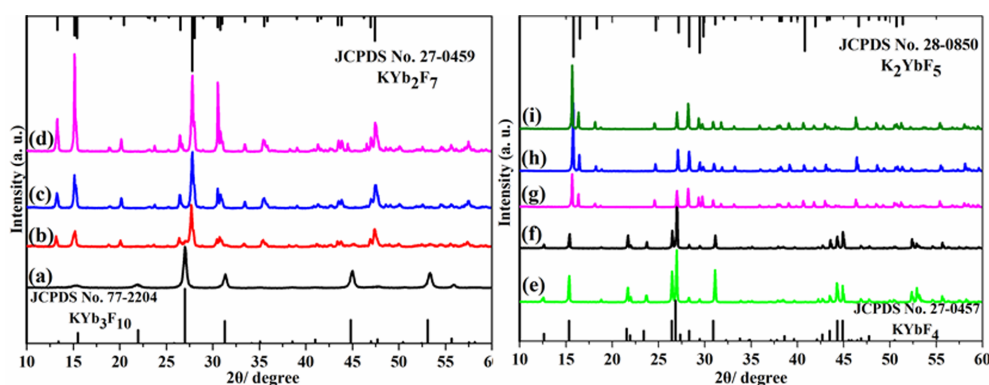


Fig. 1 XRD patterns of potassium ytterbium fluoride samples synthesized with different molar ratio of KF to Yb^{3+} : (a) $\text{KF}/\text{Yb}^{3+} = 3$, (b) $\text{KF}/\text{Yb}^{3+} = 5$, (c) $\text{KF}/\text{Yb}^{3+} = 10$, (d) $\text{KF}/\text{Yb}^{3+} = 12.5$, (e) $\text{KF}/\text{Yb}^{3+} = 15$, (f) $\text{KF}/\text{Yb}^{3+} = 20$, (g) $\text{KF}/\text{Yb}^{3+} = 40$, (h) $\text{KF}/\text{Yb}^{3+} = 50$, and (i) $\text{KF}/\text{Yb}^{3+} = 60$. The standard data of $\text{KYb}_3\text{F}_{10}$ (JCPDS No. 77-2204), KYb_2F_7 (JCPDS No. 27-0459), KYbF_4 (JCPDS No. 27-0457) and K_2YbF_5 (JCPDS No. 28-0850) are given as references.

Fig. 2 shows the typical TEM and SEM images of the samples prepared with different molar ratios of KF to Yb^{3+} . It is obvious that the as-synthesized products present remarkably different morphologies. At low molar ratio of KF to Yb^{3+} ($\text{KF}/\text{Yb}^{3+} = 3$), the TEM image in Fig. 2a reveals that cubic $\text{KYb}_3\text{F}_{10}$ consists of nanoplates with 36 nm in diameter. When the molar ratio of KF to Yb^{3+} is set as 5, KYb_2F_7 nanoparticles with average diameter about 17 nm can be obtained, as shown in Fig. 2b. At $\text{KF}/\text{Yb}^{3+} = 10$, the general image of KYb_2F_7 sample is shown in Fig. 2c. It clearly indicates that the product is composed of a mixture of hexagonal sub-microplates with average diameter about 111 nm and some nanoparticles attached on the surface. With the increase of KF/Yb^{3+} molar ratio up to 12.5, the as-prepared KYb_2F_7 product is composed of relatively uniform sub-microrods, of which the mean length is about 151 nm and average diameter is about 80 nm (Fig. 2d). Obviously, a small change in KF dosage results in the dramatic change in morphology and size of the

as-synthesized crystals, which could be related to the different characteristic unit cell structures for different crystallographic phases.^{31,32} At a medium molar ratio of KF to Yb³⁺ (KF/Yb³⁺ = 15), the regular micro-polyhedrons with average size of 6.6 μm in thickness and 40.5 μm in diameter are observed from Fig. 2e. Interestingly, the magnified SEM image (inset in Fig. 2e) demonstrates the presence of concave centers on the top/bottom surfaces. When the experiment is performed at KF/Yb³⁺ = 20, the morphology of the as-obtained sample is the micro-polyhedrons with smooth surfaces, noticeable uniformity and good monodispersity, as shown in Fig. 2f. Analysis of a number of the micro-polyhedrons indicates that these microcrystals have an average size of 23.7 μm in diameter and 46.9 μm in length. As the molar ratio of KF to Yb³⁺ rises to 40, the as-synthesized sample presents prisms morphology with trilobal cross section, as illustrated in Fig. 2g. It can be calculated that the average length is about 12.1 μm and the thickness is about 2.6 μm. More careful examination of the magnified SEM image (inset in Fig. 2g) confirms that the microprisms have shapely trilobal structure. When the KF/Yb³⁺ molar ratio reaches to 50, the sample is of a great deal of microrods with uniform size of 11.3 μm in length and 4.5 μm in diameter (Fig. 2h). The magnified SEM image (inset in Fig. 2h) displays a close-up view of one-isolated microrod, which clearly exhibits a spindle-like morphology with coarse surfaces. At high molar ratio of KF to Yb³⁺ (KF/Yb³⁺ = 60), the morphology of the as-obtained sample varies greatly. It can be clearly seen from Fig. 2i that there are a large quantity of microspheres with smooth and flat surfaces. The mean size of the sample is estimated to be about 5.2 μm in diameter. Based on the above analysis, it is obvious that the morphology of the as-obtained products can be tuned from nanoplates, nanoparticles, sub-microplates, sub-microrods, micro-polyhedrons, microprisms, microrods to microspheres by changing the molar ratio of KF to Yb³⁺. The corresponding phases, morphologies and dimensions of the products synthesized at different molar ratios of KF to Yb³⁺ are summarized in Table 1.

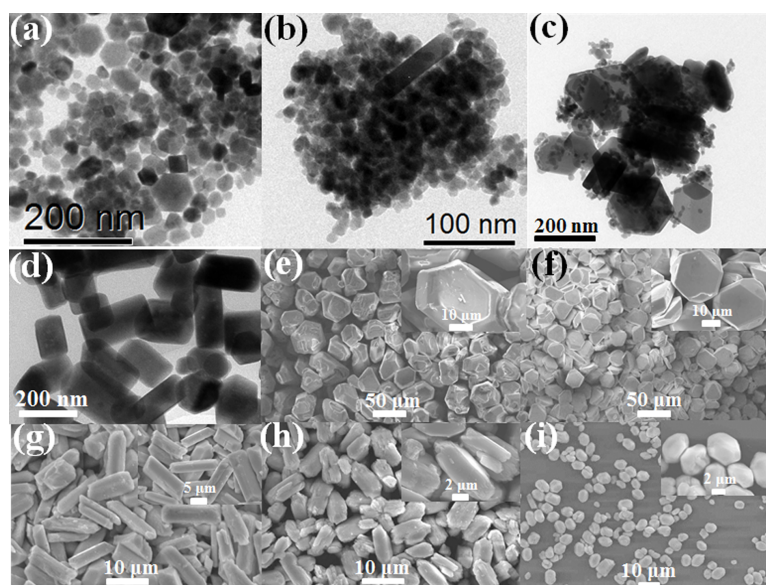


Fig. 2 TEM and SEM images of potassium ytterbium fluoride samples synthesized with different molar ratio of KF to Yb³⁺: (a) KF/Yb³⁺ = 3, (b) KF/Yb³⁺ = 5, (c) KF/Yb³⁺ = 10, (d) KF/Yb³⁺ = 12.5, (e) KF/Yb³⁺ = 15, (f) KF/Yb³⁺ = 20, (g) KF/Yb³⁺ = 40, (h) KF/Yb³⁺ = 50, and (i) KF/Yb³⁺ = 60.

Table 1 Summary of the experiment conditions and corresponding phases, morphologies and sizes of the as-synthesized samples.^a

Sample	KF:Yb ³⁺	Crystallographic phase	Morphology	Size
KYBF-1	3	Cubic KYb ₃ F ₁₀	Nanoplates	36 ± 7 nm
KYBF-2	5	Orthorhombic KYb ₂ F ₇	Nanoparticles	17 ± 2 nm
KYBF-3	10	Orthorhombic KYb ₂ F ₇	Sub-microplates + nanoparticles	111 ± 9 nm
KYBF-4	12.5	Orthorhombic KYb ₂ F ₇	Sub-microrods	(151 ± 6 nm) × (80 ± 3 nm)
KYBF-5	15	Hexagonal KYbF ₄	Micro-polyhedrons	(40.5 ± 2.6 μm) × (6.6 ± 0.5 μm)
KYBF-6	20	Hexagonal KYbF ₄	Micro-polyhedrons	(23.7 ± 1.1 μm) × (46.9 ± 3.9 μm)
KYBF-7	40	Orthorhombic K ₂ YbF ₅	Microprisms	(12.1 ± 0.9 μm) × (2.6 ± 0.3 μm)
KYBF-8	50	Orthorhombic K ₂ YbF ₅	Microrods	(11.3 ± 1.4 μm) × (4.5 ± 0.2 μm)
KYBF-9	60	Orthorhombic K ₂ YbF ₅	Microspheres	5.2 ± 0.3 μm

^a All samples were hydrothermally treated at 220 °C for 24 h.

3.2 Growth mechanism

Cite this: DOI: 10.1039/c0xx00000x

www.rsc.org/xxxxxx

ARTICLE TYPE

To shed light on the formation process of potassium ytterbium fluorides with different crystal phases and morphologies, reaction samples were carefully investigated by quenching the reaction at different time intervals. Here, K_2YbF_5 microrods are used as representative to investigate the phase and shape evolution in detail. Fig. 3 shows the XRD patterns of the K_2YbF_5 sample prepared with 50:1 KF/Yb^{3+} at different reaction times as well as standard data of orthorhombic K_2YbF_5 (JCPDS No. 28-0850) for comparison. As shown, all three samples exhibit diffraction patterns corresponding to the orthorhombic phase of K_2YbF_5 , indicating that the crystal phase of the products obtained under the similar conditions still remains the orthorhombic structure at different reaction time. Remarkably, the intensity of diffraction peaks increases significantly with the extended reaction time, implying that the crystallinity of the sample becomes higher and higher.

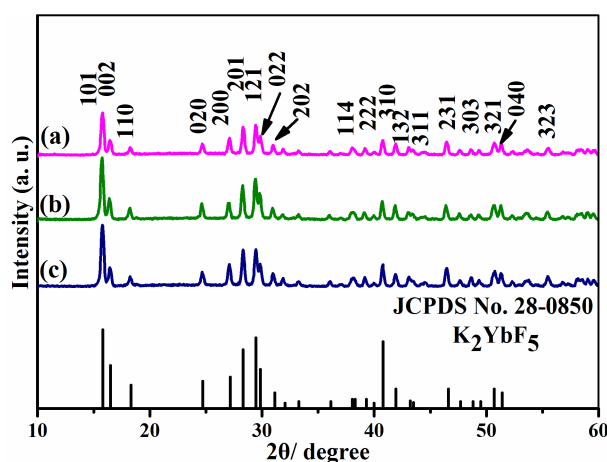


Fig. 3 XRD patterns for K_2YbF_5 microcrystals as a function of reaction time: (a) 3 h, (b) 12 h, (c) 24 h. The standard data of K_2YbF_5 (JCPDS No. 27-0457) is given as a reference.

At the same time, the morphology evolution of K_2YbF_5 crystals is carefully investigated by quenching the reaction at different time intervals. Although we know that the reaction doesn't stop immediately after the autoclave is removed from the heater because of heat transfer, we do believe that the sample obtained at that time represents certain stage in the reaction process. Fig. 4 shows the typical SEM images of the corresponding intermediate samples synthesized at different reaction stage. It is worth mentioning that the three samples present notably different morphologies in the crystal growth process. At a short reaction time of 3 h, the as-obtained sample is composed of spherical microparticles and some larger microrods (Fig. 4a). Careful observation from Fig. 4b reveals that a large amount of microparticles are attached on the surfaces of microrods. With the further reaction, from 3 h to 12 h, the fraction of microrods increases remarkably. As can be seen from Fig. 4c and 4d, relatively uniform microrods as well as a small amount of microparticles can be clearly observed. As the reaction time extended to 24 h, the microparticles disappear completely and only microrods exist, as shown in Fig. 4e and 4f, respectively. The corresponding morphology is fairly uniform microrods with average length and diameter of 11.8 μm and 4.9 μm , respectively. Based on the above results, a possible morphology evolution is demonstrated in Fig. 4g and described as follows.³² At the beginning, the solution containing oleic acid, KOH and ethanol is continuously agitated and potassium oleate (RCOOK) is generated from oleic acid (OA) and potassium hydroxide (KOH). In this procedure, two phases have formed, including the solid phase containing RCOOK and the liquid phase consisting of the redundant OA and ethanol, which further assemble to reverse micelles. Together with K^+ , OA and water, these reverse micelles can construct a microemulsion system. Because the carboxy groups of oleic acid are typically electron donors, oleate anions ($R\text{-COO}^-$) can coordinate with electron-poor metal atoms.³³ So, the oleate anions and Yb^{3+} cations are mixed with desired amount in the reverse micelles, resulting in the formation of a $(\text{RCOO})_3\text{Yb}$ complex through strong coordination interaction. Under high temperature and high pressure conditions, the chelating ability of the complexes could be weakened and the Yb^{3+}

ions are released into the reaction solution gradually. Then, K^+ and F^- ions can react with Yb^{3+} ions to generate small nuclei. At a short reaction time, these nuclei could only grow into K_2YbF_5 microparticles via the homogeneous nucleation process. With the further reaction, a dissolution-reconstruction process takes place, resulting in the formation of K_2YbF_5 microrods with the disappearance of K_2YbF_5 microparticles. As a result, there is no change in the morphology but the size of the microrods increases with the increment of reaction time.

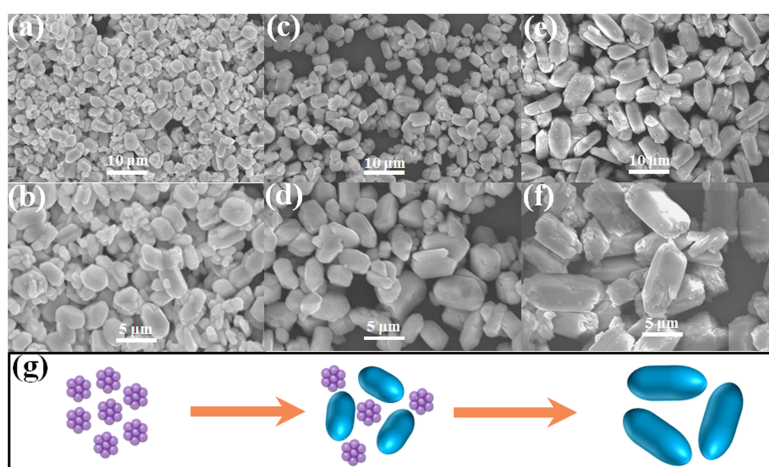


Fig. 4 SEM images for K_2YbF_5 microcrystals as a function of reaction time: (a and b) 3 h, (c and d) 12 h, (e and f) 24 h; (g) Schematic illustration for the possible formation process of K_2YbF_5 sample.

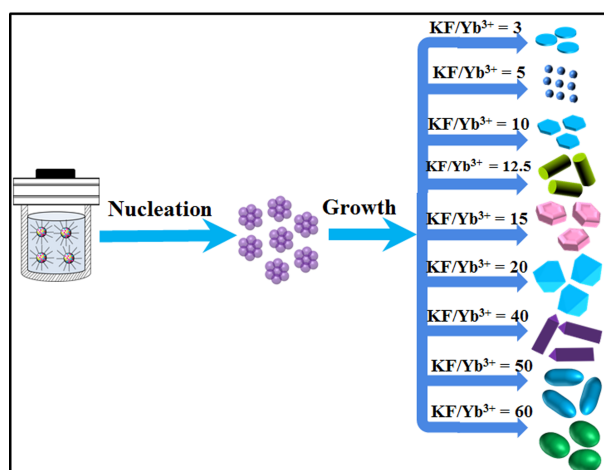
Obviously, the molar ratio of KF to Yb^{3+} has a significant influence on the crystallographic phases, morphologies and sizes of the final products. In other word, potassium ytterbium fluorides with controllable morphologies, tunable sizes and predictable phases can be successfully synthesized by simply tuning the KF dosage. Although the exact reason is not very clear at present, the explanation for the variation of morphology, size and phase could be provided as follows. The formation process of potassium ytterbium fluorides nano-/microcrystals can be described as follows: nucleation stage and crystal growth stage. At the early stage, the RCOOK is first generated from OA and KOH, resulting in the formation of reverse micelles. These reverse micelles, together with KF, OA, ethanol and water, form a microemulsion. Through strong coordination interaction, an ion exchange process happens between RCOOK and Yb^{3+} ions, leading to the formation of complexes $((RCOO)_3Yb)$. The chelating ability of $(RCOO)_3Yb$ complexes could be weakened under the conditions of high temperature and high pressure, resulting that Yb^{3+} ions would be released gradually into the reaction solution. As a result, the concentration of free Yb^{3+} ions in solution could be precisely controlled, which thus helps to control the nucleation and subsequent growth of the crystals. After the addition of the aqueous solution containing F^- ions, the oleic acid capped Yb^{3+} reacts with K^+ and F^- ions quickly to generate small nuclei. In a very short reaction time, the nuclei can grow into potassium ytterbium fluorides seeds. It has been reported that the growth of the as-synthesized potassium ytterbium fluorides are started with the reaction between F^- ions and ytterbium oleate complex $((RCOO)_3Yb)$. High F^- concentration can significantly accelerate the particle nucleation rate. A much faster nucleation speed results in a thermodynamically determined reaction process.³⁴ So, the phase synthesized at high F^- concentration is more thermodynamically stable than the phase obtained with low F^- content. With the increase of KF dosage, the nucleation rate can be significantly accelerated, resulting in a thermodynamically determined reaction process. Therefore, the corresponding thermodynamically stable phase of potassium ytterbium fluorides can be formed (thermodynamic stability: $KYb_3F_{10} < KYb_2F_7 < KYbF_4 < K_2YbF_5$). As a consequence, the crystallographic phase of potassium ytterbium fluorides changes from cubic KYb_3F_{10} , orthorhombic KYb_2F_7 , hexagonal $KYbF_4$ to more thermodynamically stable orthorhombic K_2YbF_5 . Remarkably, the phase transformation results in the dramatic morphology change of the crystals, which can be attributed to the intrinsic crystallographic structures of initial seeds. When the crystalline phase is determined, the characteristic unit cell structures of potassium ytterbium fluorides seeds greatly affect the further crystal growth. The cubic KYb_3F_{10} seeds have isotropic unit cell structures, which usually induce the isotropic growth of particles, leading to wafer-like particles. By comparison, the other potassium ytterbium fluorides seeds, including orthorhombic KYb_2F_7 , hexagonal $KYbF_4$ and orthorhombic K_2YbF_5 , have anisotropic unit cell structures, which can induce anisotropic growth along

Cite this: DOI: 10.1039/c0xx00000x

www.rsc.org/xxxxxx

ARTICLE TYPE

crystallographically reactive directions, resulting in the formation of potassium ytterbium fluorides with various morphologies, such as sub-microrods, sub-microplates, microprisms, micro-polyhedrons and microspheres. Except for the inherent crystal structure of seeds, the shape evolutions of nano-/microcrystals are also influenced by external factors such as reaction temperature, pH values in the initial solution and the reactants proportion. In this experiment, the subsequent crystal growth process of potassium ytterbium fluorides crystals is dramatically dependent on the reaction condition (the molar ratios of KF to Yb^{3+}) after the formation of crystal nucleus. Therefore, the microarchitectures and sizes of the final samples have been greatly affected by the change of KF dosage. The reason for that might be explained on the basis of the difference of the capping effect of F^- ions on the different crystal planes of growing potassium ytterbium fluoride crystals. According to the Gibbs-Thompson theory, the relative chemical potential of each crystal face is merely proportion to its surface-atom ratio, determined by the average number of dangling bonds per atom over the entire crystal planes.^{35, 36} The capping effect of F^- ions on the surface of crystal faces could change the average number of dangling bonds and further alter the chemical potential of the crystal faces. Detailed observation on the crystal structures of KYb_2F_7 , KYbF_4 and K_2YbF_5 indicates that the Yb^{3+} density on different crystal faces is various. As a result, the selective adsorption ability of F^- on various crystal panes differ from each other because of the strong coordination effect between F^- and Yb^{3+} ions. So the chemical potential of different crystal faces varies, which induces the change of the relative growth rate on different directions. According to the general principle of crystal growth, the growth rate is relate to the relative growth of different crystal facets and the different growth rate of various crystal planes results in diverse appearance of the crystallite.^{37, 38} In this present situation, the different KF dosage used in this system has a significant effect on the selective adsorption of F^- ions onto the various surfaces of growing potassium ytterbium fluoride crystals, which cause the relative growth rate on different directions changing accordingly, resulting in the formation of potassium ytterbium fluorides with different crystal morphologies and sizes. The possible formation mechanism of potassium ytterbium fluorides with different crystallographic phase, morphologies and sizes under different experimental conditions are shown in Scheme 1.



Scheme 1. Schematic illustration for the possible formation process of potassium ytterbium fluoride samples synthesized with different molar ratios of KF to Yb^{3+} .

3.3 UC luminescence properties

Here, Er^{3+} is selected as dopant ion to investigate the UC luminescence properties of potassium ytterbium fluorides with different crystallographic phases, morphologies and sizes. According to the above results, Er^{3+} ions doped potassium ytterbium fluorides with four crystalline phases, including $\text{KYb}_3\text{F}_{10}$, KYb_2F_7 , KYbF_4 and K_2YbF_5 , can be successfully synthesized by tuning the molar ratios of KF to Ln^{3+} ($\text{Ln} = \text{Yb}, \text{Er}$). For clarity, $\text{KYb}_3\text{F}_{10}:2\%\text{Er}^{3+}$, $\text{KYb}_2\text{F}_7:2\%\text{Er}^{3+}$, $\text{KYbF}_4:2\%\text{Er}^{3+}$ and $\text{K}_2\text{YbF}_5:2\%\text{Er}^{3+}$ prepared with the KF/Ln^{3+} molar

ratios of 3, 12.5, 20 and 50, are denoted as sample S1, S2, S3 and S4, respectively. From the XRD patterns and SEM images of these four samples (Fig. S11 and Fig. S12), it can be drawn that Er^{3+} ions could be doped into potassium ytterbium fluoride lattices completely and the doping has little effect on the crystal phases and morphologies. Furthermore, the EDS spectra of these samples also confirm the presence of K, Yb, Er and F elements, and the atomic ratios of K/Yb/Er/F are much close to the theoretical values (Fig. S13 and Table S11). Fig. 5 shows the UC emission spectra of S1, S2, S3 and S4 upon 980 nm laser diode excitation. It can be clearly seen that the four samples exhibit the same emission peaks yet with quite different emission intensities. As shown in Fig. 5a, the dominated red emission centered at 656 nm can be assigned to the ${}^4\text{F}_{9/2} \rightarrow {}^4\text{I}_{15/2}$ transition, and the green emissions at 521 and 542 nm account for the ${}^2\text{H}_{11/2}, {}^4\text{S}_{3/2} \rightarrow {}^4\text{I}_{15/2}$ transitions.^{20, 39} To further compare the luminescence intensity of these products, the integrated intensities of red emission for sample S1, S2, S3 and S4 are presented in Fig. 5b. Remarkably, the relative emission intensities of S1, S2, S3 and S4 differ from each other under the same measurement conditions. The ranking of the emission intensities for these samples is $\text{S1} < \text{S2} < \text{S3} < \text{S4}$. Evidently, $\text{K}_2\text{YbF}_5:2\%\text{Er}^{3+}$ microrods (S4) have the strongest emission intensity, while $\text{KYb}_3\text{F}_{10}:2\%\text{Er}^{3+}$ nanoparticles (S1) exhibit the lowest emission intensity. Moreover, the relative intensity of the former is about 15 times higher than that of the latter. To visualize the difference between the four samples, the photographs of UC emissions for S1, S2, S3 and S4 under 980 nm laser excitation are provided in Fig. 5c. The red emission of these samples with different intensities could be clearly seen by the naked eye. Obviously, S4 presents the strongest emission, agreeing well with the results in Fig. 5a and 5b. It is worth mentioning that the emission colors of these four samples keep unchanged with the variation of the incident laser power (Fig. S14). The proposed UC mechanism in the Er^{3+} doped potassium ytterbium fluorides ($\text{KYb}_3\text{F}_{10}$, KYb_2F_7 , KYbF_4 and K_2YbF_5) is shown in Fig. 5d. Based on this, the explanation for the dominated red emission can be provided as follows.^{40, 41} When a small amount of Er^{3+} (2 mol%) is doped in potassium ytterbium fluoride host matrixes, the inter-atomic distance between Yb and Er is very short, so that the back-energy-transfer from Yb^{3+} to Er^{3+} could be facilitated (${}^4\text{F}_{7/2}(\text{Er}^{3+}) + {}^2\text{F}_{7/2}(\text{Yb}^{3+}) \rightarrow {}^4\text{I}_{11/2}(\text{Er}^{3+}) + {}^2\text{F}_{5/2}(\text{Yb}^{3+})$). Subsequently, the population of Er^{3+} ions in the excited levels of ${}^2\text{H}_{11/2}$ and ${}^4\text{S}_{3/2}$ may be suppressed, leading to the decrease of green emission. Meanwhile, the energy transfer from Yb^{3+} to Er^{3+} also induce to the saturation of the ${}^4\text{I}_{3/2}$ state of Er^{3+} and then the excited Yb^{3+} ions transfer its energy to Er^{3+} ions via the energy transfer process (${}^4\text{I}_{3/2}(\text{Er}^{3+}) + {}^2\text{F}_{5/2}(\text{Yb}^{3+}) \rightarrow {}^4\text{F}_{9/2}(\text{Er}^{3+}) + {}^2\text{F}_{7/2}(\text{Yb}^{3+})$), which directly populates the ${}^4\text{F}_{9/2}$ level of Er^{3+} ions, resulting in the enhancement of red emission. The above results are consistent with the previous reports of the ytterbium-based crystals doped with Er^{3+} ions.

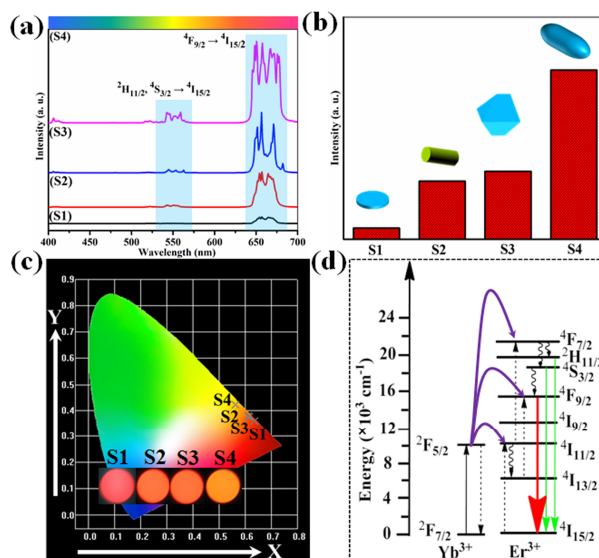


Fig. 5 (a) Room temperature UC emission spectra of sample S1, S2, S3 and S4 under 980 nm laser excitation; (b) the integrated intensity of red emission; (c) luminescent photographs and corresponding CIE chromaticity coordinates; (d) Proposed energy transfer mechanism in the Er^{3+} ions (2 mol%) doped potassium ytterbium fluorides.

Fig. 6 shows the emission decay curves of ${}^4\text{F}_{9/2} \rightarrow {}^4\text{I}_{15/2}$ (656 nm) for the four samples under 980 nm laser excitation. The effective experimental lifetime (τ_{eff}) can be calculated by using⁴²

Cite this: DOI: 10.1039/c0xx00000x

www.rsc.org/xxxxxx

ARTICLE TYPE

$$\tau_{\text{eff}} = \int [I(t) * t * dt] / \int [I(t) * dt] \quad (1)$$

where $I(t)$ represents the emission intensity at time t after the cutoff of the excitation light. The lifetimes of the ${}^4\text{F}_{9/2}$ state for S1, S2, S3 and S4 are determined to be 0.29, 0.36, 0.69 and 0.83 ms, respectively. It is obvious that the variation tendency of the lifetime corresponds well with the change of UC emission intensity. It is well-known that the measured lifetime of an excited state (τ_m) is determined by the radiative transition rate ($1/\tau_R$) and nonradiative relaxation rate (W_{NR}), which can be expressed as follows⁴³

$$1/\tau_m = 1/\tau_R + W_{\text{NR}} \quad (2)$$

The radiative transition rate is significantly influenced by the local crystal field of host lattice around the dopant, while the factors, including internal crystalline defects, surface defects and surface-associated ligands, have a great effect on nonradiative relaxation rate. Owing to the different crystal structures, morphologies and sizes of potassium ytterbium fluorides, the radiative transition rate and nonradiative relaxation rate change simultaneously with the sample accordingly. Therefore, the UC luminescence of potassium ytterbium fluorides can be dramatically influenced by one or more of the following factors: crystal phase, morphology and size. Although these four samples (S1, S2, S3 and S4) with different phases, morphologies and sizes exhibit much different UC emission intensity, it is difficult for us to discuss it in more detail. In order to compare the UC luminescence of potassium ytterbium fluorides with four crystalline phases, some preconditions including crystal morphologies, sizes and surfactants, should be under consideration. In a word, the different emission intensities among S1, S2, S3 and S4 samples may be caused by quite a few factors and will not be discussed here in more detail. Further research is also needed to investigate the UC luminescence properties of potassium ytterbium fluorides with four crystal structures.

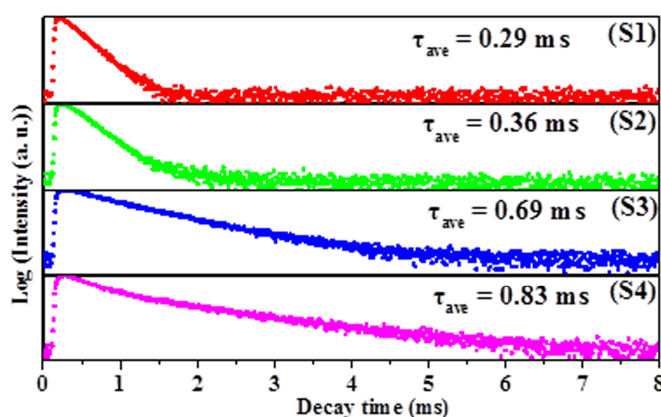


Fig. 6 Decay profiles of ${}^4\text{F}_{9/2} \rightarrow {}^4\text{I}_{15/2}$ (656 nm) transition of S1, S2, S3 and S4 under 980 nm laser excitation.

4 Conclusion

In summary, uniform potassium ytterbium fluorides with different crystallographic phases, various morphologies and sizes have been successfully synthesized by a facile and general solution-based approach. Through the simple manipulation of the molar ratio of KF to Yb^{3+} , we obtained $\text{KYb}_3\text{F}_{10}$ nanoparticles, KYb_2F_7 sub-microplates, sub-microrods, KYbF_4 micro-polyhedrons, K_2YbF_5 microprisms, microrods and microspheres. The phase and morphology evolution as well as the possible formation mechanism for the as-obtained samples with diverse crystal phases and architectures are presented in detail. In addition, the UC luminescence properties of 2 mol% Er^{3+} doped potassium ytterbium fluorides with four crystalline phases ($\text{KYb}_3\text{F}_{10}$, KYb_2F_7 , KYbF_4 and K_2YbF_5) have been systematically investigated under 980 nm laser excitation. More importantly, these results not only provide a facile and general route to modulate the crystallographic phases, morphologies and sizes of potassium ytterbium fluorides, but also assist in the crystal design and morphology-controllable synthesis of other rare earth fluoride compounds.

Acknowledgment

This project has been financially supported by Zhejiang Provincial Natural Science Foundation of China (LQ15E020004, LR15E020001 and LQ14E020006), the National Natural Science Foundation of China (61372025 and 21271170), the 151 talent's projects in the second level of Zhejiang Province and college students' activities of science and technology innovation in Zhejiang Province (2015R407033).

5 Notes and references

^a College of Materials & Environmental Engineering, Hangzhou Dianzi University, Hangzhou, 310018 P. R. China

^b Key Lab of Advanced Transducers and Intelligent Control System, Ministry of Education and Shanxi Province, College of Physics and Optoelectronics, Taiyuan University of Technology, Taiyuan 030024, P. R. China

¹⁰ ^c College of Electronic Information and Engineering, Hangzhou Dianzi University, Hangzhou, 310018 P. R. China

E-mail address: dqchen@hdu.edu.cn (D. Chen), huangxy04@126.com (X. Huang).

†Electronic Supplementary Information (ESI) available: [details of any supplementary information available should be included here]. See DOI: 10.1039/b000000x/

- 15 1. J. Pichaandi and F. C. J. M. van Veggel, *Coordin. Chem. Rev.*, 2014, 263–264, 138-150.
2. C. Li and J. Lin, *J. Mater. Chem.*, 2010, 20, 6831-6847.
3. G. Wang, Q. Peng and Y. Li, *Accounts Chem. Res.*, 2011, 44, 322-332.
4. F. Wang and X. Liu, *Chem. Soc. Rev.*, 2009, 38, 976-989.
5. M. A. El-Sayed, *Accounts Chem. Res.*, 2001, 34, 257-264.
- 20 6. J. Yang, C. Li, Z. Quan, C. Zhang, P. Yang, Y. Li, C. Yu and J. Lin, *J. Phys. Chem. C*, 2008, 112, 12777-12785.
7. Y. Zhang, X. Li, Z. Hou and J. Lin, *Nanoscale*, 2014, 6, 6763-6771.
8. X. Teng, Y. Zhu, W. Wei, S. Wang, J. Huang, R. Naccache, W. Hu, A. I. Y. Tok, Y. Han, Q. Zhang, Q. Fan, W. Huang, J. A. Capobianco and L. Huang, *J. Am. Chem. Soc.*, 2012, 134, 8340-8343.
9. Y. Zheng, J. Liu, J. Liang, M. Jaroniec and S. Z. Qiao, *Energ Environ. Sci.*, 2012, 5, 6717-6731.
- 25 10. S. Xiong, C. Yuan, X. Zhang, B. Xi and Y. Qian, *Chem. Eur. J.*, 2009, 15, 5320-5326.
11. D. Pan, S. Jiang, L. An and B. Jiang, *Adv. Mater.*, 2004, 16, 982-985.
12. E. Downing, L. Hesselink, J. Ralston and R. Macfarlane, *Science*, 1996, 273, 1185-1189.
13. G. Yi, H. Lu, S. Zhao, Y. Ge, W. Yang, D. Chen and L. H. Guo, *Nano Lett.*, 2004, 4, 2191-2196.
14. R. Deng, F. Qin, R. Chen, W. Huang, M. Hong and X. Liu, *Nat Nanotech.*, 2015, 10, 237-242.
- 30 15. A. Shalav, B. S. Richards, T. Trupke, K. W. Krämer and H. U. Güdel, *Appl. Phys. Lett.*, 2005, 86, 013505.
16. W. Wang, M. Ding, C. Lu, Y. Ni and Z. Xu, *Appl. Catal. B: Environ.*, 2014, 144, 379-385.
17. N. Rakov and G. S. Maciel, *Sensor. Actuat. B: Chem.*, 2012, 164, 96-100.
18. J. Liu, J. Bu, W. Bu, S. Zhang, L. Pan, W. Fan, F. Chen, L. Zhou, W. Peng and K. Zhao, *Angew. Chem. Int. Ed.*, 2014, 53, 4551-4555.
- 35 19. J. A. Capobianco, F. Vetrone, J. C. Boyer, A. Speghini and M. Bettinelli, *J. Phys. Chem. B*, 2002, 106, 1181-1187.
20. M. Ding, C. Lu, L. Cao, Y. Ni and Z. Xu, *Opt. Mater.*, 2013, 35, 1283-1287.
21. A. Yin, Y. Zhang, L. Sun and C. Yan, *Nanoscale*, 2010, 2, 953-959.
22. S. Heer, O. Lehmann, M. Haase and H.-U. Güdel, *Angew. Chem. Int. Ed.*, 2003, 42, 3179-3182.
23. Y. Yang, C. Mi, F. Jiao, X. Su, X. Li, L. Liu, J. Zhang, F. Yu, Y. Liu and Y. Mai, *J. Am. Ceram. Soc.*, 2014, 97, 1769-1775.
- 40 24. K. W. Krämer, D. Biner, G. Frei, H. U. Güdel, M. P. Hehlen and S. R. Lüthi, *Chem. Mater.*, 2004, 16, 1244-1251.
25. X. Zhang, P. Yang, C. Li, D. Wang, J. Xu, S. Gai and J. Lin, *Chem. Commun.*, 2011, 47, 12143-12145.
26. J. Wang, R. Deng, M. A. MacDonald, B. Chen, J. Yuan, F. Wang, D. Chi, T. S. Andy Hor, P. Zhang, G. Liu, Y. Han and X. Liu, *Nat. Mater.*, 2014, 13, 157-162.
27. C. Li, Z. Xu, D. Yang, Z. Cheng, Z. Hou, P. Ma, H. Lian and J. Lin, *CrystEngComm*, 2012, 14, 670-678.
- 45 28. H. Schäfer, P. Ptacek, O. Zerzouf and M. Haase, *Adv. Funct. Mater.*, 2008, 18, 2913-2918.
29. J. Méndez-Ramos, P. Acosta-Mora, J. C. Ruiz-Morales and N. M. Khaidukov, *J. Alloys Compd.*, 2013, 575, 263-267.
30. C. Sassoie, G. Patriarche and M. Mortier, *Opt. Mater.*, 2009, 31, 1177-1183.
31. C. Li, J. Yang, Z. Quan, P. Yang, D. Kong and J. Lin, *Chem. Mater.*, 2007, 19, 4933-4942.
32. M. Ding, C. Lu, Y. Song, Y. Ni and Z. Xu, *CrystEngComm*, 2014, 16, 1163-1173.
- 50 33. F. Zhang, Y. Wan, T. Yu, F. Zhang, Y. Shi, S. Xie, Y. Li, L. Xu, B. Tu and D. Zhao, *Angew. Chem. Int. Ed.*, 2007, 46, 7976-7979.
34. W. Bu, B. Chen, L. Wang, J. Wu, X. Teng, R. Lau, L. Huang and W. Huang, *nanoscale*, 7, 4048-4054.
35. S. H. Yu, B. Liu, M. S. Mo, J. H. Huang, X. M. Liu and Y. T. Qian, *Adv. Funct. Mater.*, 2003, 13, 639-647.
36. X. Liang, X. Wang, J. Zhuang, Q. Peng and Y. Li, *Adv. Funct. Mater.*, 2007, 17, 2757-2765.
37. R. Laudise, E. Kolb and A. Caporaso, *J. Am. Ceram. Soc.*, 1964, 47, 9-12.
- 55 38. C. Li, Z. Quan, J. Yang, P. Yang and J. Lin, *Inorg. Chem.*, 2007, 46, 6329-6337.
39. X. Zhang, P. Yang, C. Li, D. Wang, J. Xu, S. Gai and J. Lin, *Chem. Commun.*, 2011, 47, 12143-12145.
40. N. Niu, P. Yang, F. He, X. Zhang, S. Gai, C. Li and J. Lin, *J. Mater. Chem.*, 2012, 22, 10889-10899.
41. S. Huang, J. Xu, Z. Zhang, X. Zhang, L. Wang, S. Gai, F. He, N. Niu, M. Zhang and P. Yang, *J. Mater. Chem.*, 2012, 22, 16136-16144.
- 60 42. D. Chen, Y. Yu, Y. Wang, P. Huang and F. Weng, *J. Phys. Chem. C*, 2009, 113, 6406-6410.
43. X. Xue, S. Uechi, R. N. Tiwari, Z. Duan, M. Liao, M. Yoshimura, T. Suzuki and Y. Ohishi, *Opt. Mater. Express*, 2013, 3, 989-999.